Ion acceleration in short-pulse laser–target interactions

A. A. A N D R E E V[1] and J. L I M P O U C H[2]

[1] Institute for Laser Physics, Vavilov State Optical Institute, Birzhevaya line 12, Skt. Petersburg, Russia

[2] Faculty of Nuclear Sciences and Physical Engineering, Czech Technical University, Břehová 7, 115 19 Prague, Czech Republic

Abstract. Emission of energetic ions from solid targets irradiated by intense ultrashort laser pulses is studied in the framework of a one-dimensional self-consistent hydrodynamical model. The computed ion spectra reproduce well the basic parameters of published experimental results. Optimum conditions are found for the generation of MeV ions by picosecond laser pulses.

1. Introduction

The plasma produced when a powerful laser pulse is focused onto a target surface in vacuum can provide an intense source of highly charged energetic ions. Experimental laser ion sources have been investigated for medical physics and particle accelerator applications (Brown 1989; Sherwood 1992).

The above-mentioned studies have assumed nanosecond or subnanosecond laser pulses, while the development of T^3 (terawatt table-top) lasers has opened up opportunities for an extensive research of interactions of high-intensity ($I \approx 10^{14}$–$10^{19}\,\mathrm{W\,cm^{-2}}$) short laser pulses ($t_L \approx 100\,\mathrm{fs}$–1 ps) with solid targets. The physics of this system differs considerably from the conventional interactions of longer pulses. Plasma density scale lengths are shorter than the laser wavelength, and high-density plasmas are produced. The nonlinear character of the interaction is often apparent, and a considerable part of the laser energy is transferred to a group of very fast electrons and ions. An important advantage of T^3 lasers is their relatively high repetition rate, which is usually several hertz, but can easily be increased up to several kilohertz. Such a system may provide a relatively cheap and compact source of intense short pulses of very energetic ions, at least for small and medium ion charges.

Fast ion emission from solid targets irradiated by subpicosecond laser pulses has been observed (Meyerhofer *et al.* 1993; Andreev *et al.* 1996). In these experiments, MeV ions were detected, and relatively large efficiencies of laser energy transfer to the energetic ions were found.

Interactions of intense subpicosecond laser pulses with solid targets are now widely studied, both experimentally and theoretically; see the review article by Gibbon and Förster (1996). Various types of plasma description, including particle-in-cell (PIC), Vlasov, Fokker–Planck and hydrodynamical, are used in numeri-

cal simulations of the interactions. Hydrodynamical and Fokker–Planck simulations cannot avoid a phenomenological treatment of nonlinear regimes of laser absorption. These types of models are hardly applicable to the interactions of high-intensity ($I\lambda^2 \gtrsim 10^{18}\,\mathrm{W\,cm^{-2}\,\mu m^2}$) and/or very short ($t_L \lesssim 100\,\mathrm{fs}$) laser pulses with matter, when nonlinear and collective effects dominate. However, they are the only methods enabling global simulations of the interactions of moderate-intensity picosecond laser pulses with solid targets. Fokker–Planck simulations describe the heat flux rigorously, and they may be used for the description of X-ray emission in lines, when a non-Maxwellian electron distribution is present (Matte *et al.* 1994). On the other hand, hydrodynamical simulations are computationally less demanding and can incorporate a description of a broader spectrum of the physical processes occurring in the interaction.

We have developed a simplified, but self-contained, theoretical model that can, by means of one-dimensional hydrodynamical simulations, predict the ion energy spectrum and the efficiency of laser energy transformation to the fast ions. We assume here p-polarization of laser radiation, since it enhances fast-particle production, although the model is capable of accounting for any laser polarization. The model reproduces well the basic parameters of the published experimental results (Meyerhofer *et al.* 1993; Andreev *et al.* 1996), and it enables us to analyse the impact of various laser and target parameters on the fast-ion emission.

The model benefits from earlier papers describing the interactions of laser pulses with solid targets. A remarkably precise description of resonance absorption and of electron acceleration was developed some time ago (Andreev *et al.* 1980). A simplified description of nonlinear wavebreaking is added to the model in the way proposed by Rae and Burnet (1991), which allows us to use it for higher laser intensities and shorter density scale lengths. Our treatment of fast-electron transport into the target is partly similar to that of Davis *et al.* (1995), who also studied the interaction of subpicosecond laser pulses with solid targets in the framework of a hydrodynamical model. However, their model used ad hoc assumptions about the energy and number of fast electrons. They did not present any model of ion acceleration. The treatment of ion acceleration by an ambipolar electric field is based here on a semianalytical model due to Gurevich and Mescherkin (1981).

The description of all of the above-mentioned processes is incorporated into a complex model that enables us to simulate the interactions of picosecond laser pulses with solid targets in a self-consistent way. The application of the model to an investigation of fast-ion emission from solid targets is presented here.

2. Theoretical model

The plasma dynamics is described via a one-fluid two-temperature Lagrangian hydrocode taking account of electron and ion thermal conductivities, both natural and artificial ion viscosities, and the impact of the ponderomotive force on the plasma motion. The system of hydrodynamical equations, including mass, momentum and energy conservation laws, is written down using the Lagrangian mass coordinate $s = \int_{-\infty}^{x} \rho(x')\,dx'$, as follows (Dragila and Krepelka 1978):

$$\frac{\partial}{\partial t}\left(\frac{1}{\rho}\right) = \frac{\partial}{\partial s}\,U, \tag{1a}$$

$$\frac{\partial U}{\partial t} + \frac{\partial}{\partial s}\left(P_e + P_i + \mu_e + \mu_i\right) + \frac{\mathrm{Re}(\varepsilon) - 1}{16\pi}\frac{\partial |E|^2}{\partial s} = 0, \tag{1b}$$

$$\frac{\partial x}{\partial t} = U, \tag{1c}$$

$$\frac{\partial\left(\mathscr{E}^e + \mathscr{E}^{\mathrm{ion}}\right)}{\partial t} + \left(P_e + \mu_e\right)\frac{\partial}{\partial s}U + \frac{\partial}{\partial s}q^e = \frac{1}{\rho}\left(-Q_{ei} - Q_r + Q_L + Q_f\right), \tag{1d}$$

$$\frac{\partial\mathscr{E}^i}{\partial t} + \left(P_i + \mu_i\right)\frac{\partial}{\partial s}U + \frac{\partial}{\partial s}q^i = \frac{1}{\rho}Q_{ei}. \tag{1e}$$

Here ρ and U are the plasma density and velocity, $P_{e,i}$ and $\mu_{e,i}$ are the electron and ion pressures and viscosities, $\mathscr{E}^{e,i}$ are the electron and ion thermal energies per unit mass, $q_{e,i}$ are for the electron and ion heat fluxes, Q_{ei} is the electron–ion relaxation, $\mathscr{E}^{\mathrm{ion}}$ is the energy spent on plasma ionization, E is the amplitude of the laser electric field, ε is the complex plasma dielectric constant, Q_r is the energy loss due to X-ray emission, Q_f is the energy deposed by fast electrons, and

$$Q_L = \frac{\omega_0}{8\pi}\mathrm{Im}(\varepsilon)\left(|E_l|^2 + |E_\perp|^2\right)$$

is the collisional absorption of laser radiation, where the indices l and $\perp$ indicate the longitudinal (along the density gradient) and transverse components of the laser electric field and ω_0 is the laser frequency. A very fine spatial grid with typically 200–500 cells is used to model the shape of the density profile in the expanding plasma in detail so that the laser fields may be calculated properly. A one-dimensional planar description is usually sufficient for short pulse interactions with solid targets, since the diameter of the laser focus is much greater than the scale length of the plasma expansion during the laser pulse.

A simplified model of atomic physics is included in the code, in order to calculate the mean ion charge Z and the averaged ion charge squared $\overline{Z^2}$. The populations $N^{(z)}$ of the charge states z are described via a set of atomic rate equations

$$\frac{\partial}{\partial t}\left(\frac{N^{(z)}}{n_i}\right) = \frac{\partial}{\partial t}y^{(z)} = \Gamma^{(z)}, \qquad z = 1, 2, \ldots, z_{\mathrm{nucl}}, \tag{2}$$

where the overall rates

$$\Gamma^{(z)} = s^{(z-1)}y^{(z-1)} - \left(s^{(z)} + \alpha^{(z-1)}\right)y^{(z)} + \alpha^{(z)}y^{(z+1)},$$
$$\Gamma^{(z_{\mathrm{nucl}})} = s^{(z_{\mathrm{nucl}}-1)}y^{(z_{\mathrm{nucl}}-1)} - \alpha^{(z_{\mathrm{nucl}}-1)}y^{(z_{\mathrm{nucl}})}$$

are expressed via the ionization $s^{(z)}$ and the recombination $\alpha^{(z-1)}$ rates for an ion in charge state z. The charge state of a fully stripped ion is z_{nucl}. The population of neutrals is denoted by $N^{(0)}$, and is expressed from the normalization condition

$$n_i = N^{(0)} + \sum_{i=1}^{z_{\mathrm{nucl}}}N^{(i)},$$

where n_i is the total concentration of the ionized and the neutral atoms (the ion density). The populations $N^{(z)}$ of the ion charge states are used explicitly in the description of the transport of fast electrons into the target. The rates of collisional ionization, and radiative and three-body recombination, taken from Lee *et al.* (1984), include the depression of the ionization potential in dense plasmas. The theory of Ammosov *et al.* (1986) is used for the rate of tunnelling ionization by laser radiation. For solid aluminium targets, tunnelling ionization is important

only in a very thin layer (a few angstroms) on the surface that expand so fast that collisional ionization is inefficient. Plasma recombination is important when a laser prepulse is present. Recombination has a significant impact on the time-integrated X-ray emission from the target, too. However, recombination is not important for the results presented here.

The energy loss Q_r by radiation consists of bremsstrahlung and recombination emission multiplied by the escape factor, so that only the part of emission that reaches the plasma–vacuum boundary is included in the energy conservation.

Maxwell's equations are solved in the presented model, for both s- and p-polarized laser radiation. As the description of an s-polarized laser wave, absorbed only collisionally, is straightforward, we shall concentrate here on p-polarized obliquely incident radiation. When a p-polarized wave is incident on an inhomogeneous plasma, a fraction of its energy is collisionally absorbed and a fraction of its energy is transformed to the longitudinal electron plasma wave. The energy of the longitudinal wave is fully absorbed in the plasma, either collisionally or by Landau damping or in a nonlinear way by wavebreaking. While the collisional absorption of the transverse and longitudinal waves heats the thermal electrons, the remainder of the energy of the longitudinal wave is deposited in a group of electrons, accelerated to high energies (fast electrons). Laser absorption and electromagnetic fields are calculated by numerical solving Maxwell's equations for a hot plasma:

$$\frac{d^2 H}{dx^2} - \frac{d\ln\varepsilon}{dx}\frac{dH}{dx} + \frac{\omega_0^2}{c^2}\left(\varepsilon - \sin^2\theta\right)H = -\frac{\omega_0^2}{c^2}\sin\theta\left(\varepsilon E_l + \sin\theta\, H\right), \quad (3a)$$

$$3\beta^2\frac{\omega_p^2}{\omega_0^2}\frac{d^2 E_l}{dx^2} + 2i\frac{\omega_0}{c^2}\hat{\Gamma}E_l + \frac{\omega_0^2}{c^2}\varepsilon E_l = -\frac{\omega_0^2}{c^2}\sin\theta\, H, \quad (3b)$$

where the plasma dielectric constant is

$$\varepsilon = \varepsilon(\omega_0, k = 0) = 1 - \frac{\omega_p^2}{\omega_0(\omega_0 + i\nu)},$$

ω_p and ν are the plasma frequency and the effective electron–ion collision frequency, and

$$\beta^2 = \frac{k_B T_e}{mc^2} \equiv \frac{v_T^2}{c^2}$$

is the dispersion coefficient. Instead of the laser magnetic field B_y, we use the quantity H, introduced as follows:

$$H(x) = B_y(x) + 3\,\beta^2\sin\theta\int_{-\infty}^{x}dx'\,\frac{\omega_p^2(x')}{\omega_0^2}\,\frac{dE_l(x')}{dx'}\,.$$

These equations are solved together with four boundary conditions: two in the overdense plasma and two at the plasma–vacuum boundary.

The methodology developed by Lee and More (1984) is used for the calculation of the collision frequency ν, which describes the collisional part of the laser absorption. Landau damping of the longitudinal plasma wave is described precisely by an integral operator (Andreev *et al.* 1980).

$$\hat{\Gamma}E_l(x) = \int\gamma_L(k)F_k e^{ikx}dk = \int dk\,\gamma_L(k)\int\frac{dx'}{2\pi}\,E_l(x')\,e^{ik(x-x')},$$

where the damping rate $\gamma_L(k)$ is expressed via the electron distribution function $f(v)$.

When a linear plasma density profile is assumed and the effective collision frequency ν is spatially constant, an analytical approximation can be found for the longitudinal electric field E_l. This field is expressed through the field H at the critical surface x_c:

$$E_l = -i \sin\theta \, \frac{L_c \omega_0}{v_T} H(x_c) \int_0^\infty d\tau \exp\left\{ -L_c \omega_0 \left[i \frac{x\,\tau}{v_T L_c} + \frac{i\,\tau^3}{v_T} + \frac{\nu}{\omega_0} \frac{\tau}{v_T} + \frac{\pi}{n_c} f_c\left(\frac{v_T}{\tau}\right) \right] \right\},$$

for any electron distribution f_c at the critical surface, where the electron density is n_c and L_c is the density scale length. This approximate formula is in a good agreement with the numerical results for relatively long density profiles with density scale lengths $L_c \gtrsim 0.1\lambda$.

However, solving an integro-differential equation system at each time step of the hydrodynamical code is extremely time-consuming. The complex-β^2 approximation, proposed by Andreev *et al.* (1981), is used in the hydrocode instead of the integral operator of Landau damping. An imaginary part is added to the dispersion coefficient β^2 to account for Landau damping:

$$\beta^2 = \frac{k_B T_e}{m\,c^2} \, \frac{1}{1 + i\nu_L},$$

$$\nu_L = \frac{\xi_L}{4} \max\left(\frac{n_c}{n_e} - 1, \, 0 \right).$$

The Landau-damping rate $\nu_L = 0$ for electron densities $n_e \geqslant n_c$, and ν_L is large in a low-density plasma. The coefficient ξ_L may be modified to ensure that the longitudinal wave is damped out completely before it reaches the plasma–vacuum boundary. We have verified numerically that, at least for the typical profiles of plasma parameters encountered here, the errors introduced into the absorption efficiency and into the laser fields by the complex-β^2 approximation are insignificant. The scaling of the absorption efficiency for density scale lengths less than the laser wavelength differs considerably (Andreev *et al.* 1994) from the well-known scaling for an extensive plasma expansion.

The plasma resonance is limited in a nonlinear way by so-called wavebreaking (Estabrook *et al.* 1975) for high laser intensities, when

$$\frac{v_E}{v_T} \geqslant \frac{9}{\Phi(q)} \left(\frac{L_c \, v_T^2}{\lambda^3 \, \omega_p^2} \right)^{1/6}.$$

Here v_T is the electron thermal velocity and v_E is the oscillation velocity of an electron in the laser wave, $q = (\omega_0 L_c/c)^{2/3} \sin^2\theta$ and $\Phi(q)$ is the Ginzburg function. A detailed description of the wavebreaking mechanism is possible only in the framework of a kinetic approximation. In the wavebreaking regime, a resonance is formed and destroyed in a small number of laser periods. Here the limitation on the resonance field is described in a phenomenological way, which enables us to calculate the effective values of the resonance laser fields via the stationary wave equation. Wavebreaking leads to a nonlinear limitation of the amplitude on the laser electric field at resonance.

When the resonance absorption is treated without the spatial dispersion, an effective collision frequency is introduced into the dielectric constant to account for wavebreaking (Rae and Burnet 1991). However, this has to be modified for a hot
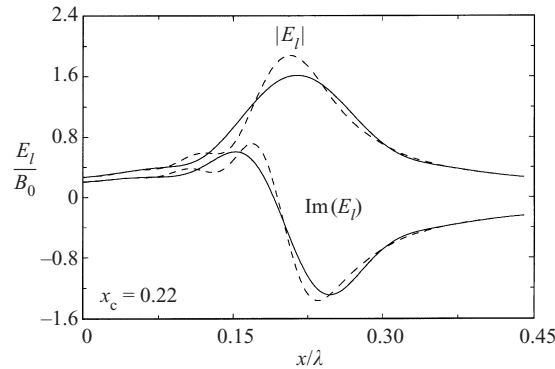
Figure 1. Profiles of the longitudinal electric field E_l (the absolute value and the imaginary component), when wavebreaking is (solid curves) and is not (dashed curves) included. A p-polarized Nd-laser wave at $I = 8.10^{15} \, \text{W cm}^{-2}$ is incident at a $45°$ angle onto an exponential plasma density profile with scale length $L_c = 0.1\lambda$ and $T_e = 0.5 \, \text{keV}$. The critical surface is located at x_c, and B_0 is the amplitude of the incident wave in vacuum.

plasma, and we introduce an effective damping rate

$$\gamma_B = \omega_0 \frac{v_c}{c} \left[\left(1 + \frac{\omega_0 L_c}{2c} \frac{v_c}{c} \right)^2 - 1 \right]^{-1/2},$$

$$v_c = \frac{e \, H(x_c)}{m \, \omega_0} \sin \theta,$$

into the equation for the longitudinal component E_l of the high-frequency electric field. The impact of wavebreaking on the laser fields is demonstrated in Fig. 1.

Vacuum heating (Brunel 1987) is not taken into account here, since the plasma density scale length is large enough to meet the condition $\omega_0 L_c \gtrsim 0.3 \, v_T$. Laser-induced surface waves may enhance laser absorption (Dragila and Gamaly 1991), but the contribution of this mechanism to laser absorption is not yet clear. Corrugations and imperfections of the target surface may dramatically enhance laser absorption at normal incidence, when the absorption efficiency in a target with a perfect surface is rather low: about 10% (Price *et al.* 1995). A possible enhancement of laser absorption is much less important for p-polarized radiation, since the absorption efficiencies are generally much higher (about 50%).

The acceleration of electrons at resonant absorption is treated in each time step via stationary electron diffusion (Andreev *et al.* 1980) in velocity space. The average diffusion coefficient $D(v)$ is expressed through the electron acceleration by the resonant Fourier component F_k of the longitudinal electric field:

$$v \frac{\partial f}{\partial x} = \frac{\partial}{\partial v} \left[D(v) \frac{\partial f}{\partial v} \right], \qquad (4)$$

where

$$D(v) = \xi_D \frac{e^2}{2 \, m^2} \frac{1}{L \, v} |F_k|^2_{k=\omega_0/v},$$

and F_k is the Fourier transform of the longitudinal electric field. Electrons are assumed to be accelerated in the plasma resonance region of width $L \approx (L_c r_{De}^2)^{1/3}$, where r_{De} is the electron Debye radius. The factor $\xi_D \approx 1$ is iterated to reach an
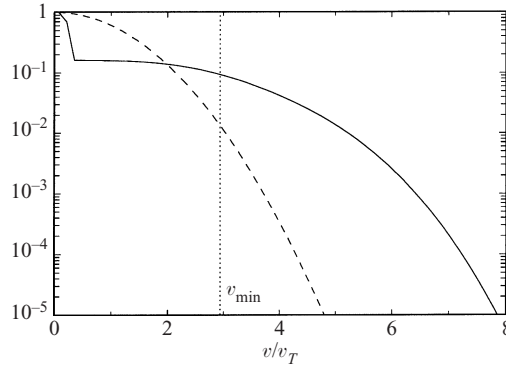
Figure 2. The Maxwellian distribution f_M of the electrons incident from the overdense plasma (dashed curve) and the distribution f_A of the electrons accelerated by resonance absorption (solid curve). The normalization is $f(v = 0) = 1$. The velocity $v_{\min}$ is the minimum velocity of the distribution function δf_A of the fast electrons. The electron spectra are displayed at the peak intensity $10^{16}\,\mathrm{W\,cm^2}$ of a p-polarized Gaussian 400 fs FWHM Nd-laser pulse incident at a $45°$ angle onto a solid aluminium target.

exact matching between the laser energy flux absorbed into the fast electrons and the energy flux of the fast electrons.

If wavebreaking is absent and Landau damping is described via the integral operator then $\xi_D = 1$ exactly. The diffusion coefficient $D(v)$ may be then expressed for linear plasma density profiles via the laser field H at the critical surface x_c:

$$D(v) = \frac{e^2}{2\,m^2}\,\frac{L_c^2}{L\,v}\,|H(x_c)|^2\,\sin^2\theta\,\exp\left\{-\frac{L_c}{r_{De}}\left[\frac{2\pi\,v_T}{n_c}\,f_c(v) + \frac{\nu(v)\,r_{De}}{v}\right]\right\}.$$

Electrons are accelerated preferentially in the direction towards the underdense plasma. The energy of the fast electrons matches the difference between the overall laser absorption and the integrated local collisional absorption, so that energy conservation is maintained. We assume here a Maxwellian distribution f_M of the electrons entering the critical region from the overdense plasma, with local temperature T_e and concentration $n_e = \alpha_f n_c$. We typically set the coefficient $\alpha_f \approx 1.5$. A typical electron distribution function $f_A(v)$ of the accelerated electrons at the vacuum side of the acceleration region is displayed in Fig. 2 at the laser pulse maximum, together with f_M. The longitudinal velocity v is oriented in the direction towards the vacuum. As the electron distribution is not modified for zero velocity ($f_A(v = 0) = f_M(v = 0)$), the distribution functions in Fig. 2 are normalized so that $f(v = 0) = 1$.

The electron distribution is split into two parts – thermal and fast electrons – in order to allow a suitable description of the energy transport into the target. We introduce the assumption that fast electrons are only those electrons carrying the net increase in energy flux density due to collisionless absorption (Landau damping and wavebreaking). The velocity $v_{\min}$, indicated by the vertical dotted line in Fig. 2, is determined by the requirement of equal energy fluxes of the electrons with $v \leqslant v_{\min}$ for the distribution functions f_A and f_M:

$$\int_0^{v_{\min}} v^3\,f_A(v)\,dv = \int_0^{v_{\min}} v^3\,f_M(v)\,dv.$$

Thus the distribution function δf_A of the fast electrons is defined here, as follows:

$$\delta f_A = \begin{cases} 0 & (v < v_{\min}), \\ f_A - f_M & (v > v_{\min}). \end{cases}$$

When the fast electrons are reflected back from the plasma–vacuum boundary, a fraction η_i of their energy is lost on acceleration of ions by an ambipolar electric field. For simplicity, η_i is assumed here to be independent of the electron velocity. The magnitude of η_i is determined by the requirement of energy conservation; the total energy lost by the fast electrons has to be equal to the energy gained by the fast ions.

The flight of fast electrons is a means of fast energy transport over relatively large distances. No net particle flux is induced, since the return current substitutes fast electrons by thermal ones everywhere to ensure quasineutrality. Fast electron transport is described simply as a continuous slowing down. The distribution function of the fast electrons reflected from the plasma–vacuum boundary, expressed via δf_A, is used as a boundary condition

$$f_f(s(x_c), v) = \frac{\delta f_A[v/(1 - \eta_i)^{1/2}]}{1 - \eta_i}$$

for solving for the transport of energetic electrons from the critical surface into the target. The longitudinal velocity v in the distribution f_f of the fast electrons in the overdense plasma is oriented into the target. The stopping power of the fast electrons is written in the Bethe–Bloch form (Davis *et al.* 1995)

$$\frac{\partial \mathscr{E}_f}{\partial s} = \frac{1}{\rho} \frac{\partial \mathscr{E}_f}{\partial x} = -\frac{2\pi e^4}{\rho \mathscr{E}_f} \left[\sum_{z=0}^{z_{\mathrm{nucl}}-1} Z_v^{(z)} N^{(z)} \ln\left(\frac{1.16\,\mathscr{E}_f}{\chi^{(z)}}\right) + n_e \ln\left(\frac{1.16\,\mathscr{E}_f}{\chi_0}\right) \right], \quad (5)$$

where $\mathscr{E}_f = \frac{1}{2}m_e v^2/2$ is the kinetic energy of a fast electron, $Z_v^{(z)}$ and $\chi^{(z)}$ are the number of valence electrons and the ionization potential of an ion in the charge state z respectively, and χ_0 is the effective potential related to the stopping power by collective processes in the plasma. The distribution function f_f is calculated in each spatial cell. Electrons that are slowed below the minimum speed v_m (usually set equal to the local thermal velocity) are assumed to be stopped within one spatial cell. The dissipated energy of fast electrons is transferred locally to the thermal electrons. The power Q_f of the thermal electron heating per unit mass is expressed as follows:

$$Q_f = -\frac{dI_f}{ds} = -\frac{d}{ds} \int_{v_m}^{\infty} v \mathscr{E}_f f_f(s, v)\, dv$$

$$= -\int_{v_m}^{\infty} \frac{d\mathscr{E}_f}{ds} v f_f(s, v)\, dv - \int_{v_m}^{\infty} \mathscr{E}_f \frac{d}{ds}\left[v f_f(s, v)\right]\, dv.$$

Here I_f is the energy flux and $f_f(s, v)$ is the distribution function of fast electrons. The first term on the right-hand side represents the energy lost by the fast electrons flying through a spatial cell, while the second term represents the energy of the fast electrons stopped there. The power Q_f leads to a precursor to the thermal wave, heating the target. The energy of the fastest electrons escaping from the simulation region into the bulk target is lost for the simulation. It is relevant for thick solid targets, where practically no fast electrons are reflected back into the interaction region. The time of flight of the fast electrons inside the simulation box

(typically $l_s \ll 10 \ \mu$m deep) is not taken into account, since it is short compared with the laser pulse duration $t_L \approx 1$ ps. A small energy, lost to K_α emission, is omitted.

Electrostatic acceleration of ions in the ambipolar field at the plasma–vacuum boundary is assumed. The fast-ion spectrum is found from the electron spectrum via the model developed by Gurevich and Mescherkin (1981). It assumes quasineutrality (density scale length much greater than the Debye radius) and that the time of fast-electron round trip in the corona is small compared with the laser pulse. These conditions are generally met in our simulations, with the exception of a small proportion of very energetic electrons penetrating far away from the target. The electron distribution is then symmetric in the longitudinal velocity v, and the electron concentration is governed by the electrostatic potential:

$$Zn_i = n_e(\varphi) = 2 \int_0^\infty f_A\left(\left(v^2 + \frac{2e\varphi}{m_e}\right)^{1/2}\right) dv, \tag{6}$$

where f_A is the above-specified distribution function of the electrons accelerated by resonance absorption. The electrostatic potential is set to $\varphi = 0$ at the critical surface and $\varphi \to \infty$ at the vacuum side ($x \to -\infty$). The evolution of ion density and velocity is then described by collisionless hydrodynamics. A self-similar solution is then applied to calculate the time-integrated energy distribution of the ions. The electron distribution f_A is averaged over the laser pulse duration to obtain a constant electron distribution for the model of ion acceleration. The ion velocity u, sound velocity c_s and electrostatic potential φ are expressed as implicit functions of the self-similar variable $\tau = x/t$ via the following set of equations:

$$u = \tau + c_s(\varphi),$$

$$c_s^2(\varphi) = \frac{eZn_e(\varphi)}{M_i}\left(\frac{dn_e}{d\varphi}\right)^{-1}$$

$$-\tau = c_s(\varphi) + \frac{eZ}{M_i}\int_0^\varphi \frac{d\varphi'}{c_s(\varphi')} \, .$$

The ion velocity distribution is then expressed via transformation of variables as follows:

$$\frac{dN}{du} = n_i\left|\frac{dx}{du}\right| \approx n_i t_L \left|\frac{d\tau}{du}\right|, \tag{7}$$

where t_L is the laser pulse duration and N is the number of ions emitted per unit surface of the target.

The function $\tau(\varphi)$ is not monotonic, when the ratio of the fast to the thermal electron temperatures is high ($\gtrsim 10$). Consequently two values of φ as a function of τ may be found (Wickens *et al.* 1978). This is related physically to the formation of a narrow layer inside the expanding plasma, where the assumption of quasineutrality no longer holds. A strong electric field inside this layer leads to a nearly stepwise acceleration of ions, which leads to a minimum in the ion energy spectrum. We introduce here a step into the function $u(\tau)$, which leads to a solution with the ion spectrum $dN/du = 0$ in an interval of ion velocities u corresponding to the rapid acceleration.
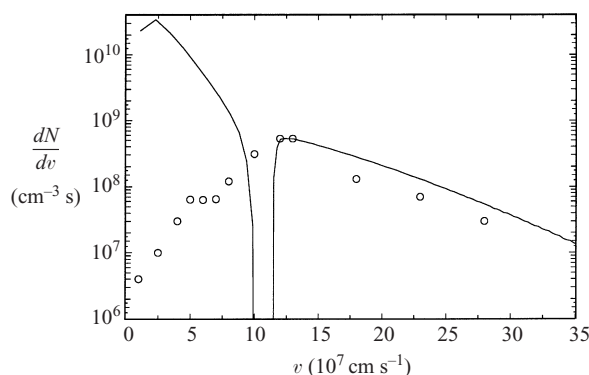
Figure 3. The spectrum of ions emitted normally from a solid Al target, irradiated by a p-polarized 1 ps FWHM Gaussian Nd-laser pulse with a peak intensity of $8 \times 10^{15}\,\mathrm{W\,cm^{-2}}$, incident at a $57°$ angle. The calculated data (curves) compared with the experimental spectrum (Meyerhofer et al. 1993) (circles).

3. Results and discussion

We have performed simulations for the conditions of the published experiments (Meyerhofer *et al.* 1993; Andreev *et al.* 1996), and the resulting spectra of fast ions are compared with the measurements. A standard transformation of the ion blowoff current traces, displayed in Fig. 2 of Meyerhofer *et al.* (1993), is performed in order to facilitate the comparison of the ion spectra with our simulations. The experimental ion spectrum and the simulation result are presented in Fig. 3. The position of the maximum of the fast-ion spectrum and also the slope of the tail of the ion spectrum compare well with the experimental data. The fast ions are confined within an angle of about $5°$ from the target normal in the experiment of Meyerhofer *et al.* (1993). As the angular distribution of the thermal ions is much broader, the discrepancy at low velocities can be explained by the geometrical factor. The total energy of the fast ions is about 20 % of the incident laser energy in the experiment of Meyerhofer *et al.* (1993), while the computed value is 9.6%. The computed laser absorption efficiency $A = 39\%$, which is lower than the experimental efficiency $A \approx 63 \pm 10\%$, may partially account for the difference in the energy transformation to the fast ions.

It should be mentioned that the completely depleted gap in the computed ion velocity spectrum is caused by the model of ion acceleration employed. This gap is present when the ratio of the fast-electron temperature T_h to the temperature T_e of the thermal electrons exceeds a certain limit. This limit is $T_h/T_e \approx 9.6$ for a bi-Maxwellian electron distribution (Wickens *et al.* 1978). No depleted gap in the ion distribution is observed in simulations of the experiments by Meyerhofer *et al.* (1993) with peak laser intensities below $5 \times 10^{15}\,\mathrm{W\,cm^{-2}}$.

We have also conducted simulations for the conditions of the experiment by Andreev *et al.* (1996). The fast-ion detector was placed $45°$ from the target normal in this experiment. Our one-dimensional model cannot describe this measurement correctly. However, the basic parameters of the computed fast-ion spectrum, shown in Fig. 4, are similar to those of the experiment. As the experimental spectrum is not absolutely calibrated, i.e. the total energy of the fast ions is not known, we normalize the experimental spectrum here, so that its maximum is equal to the maximum of the computed fast-ion distribution. The computed ion distribution is
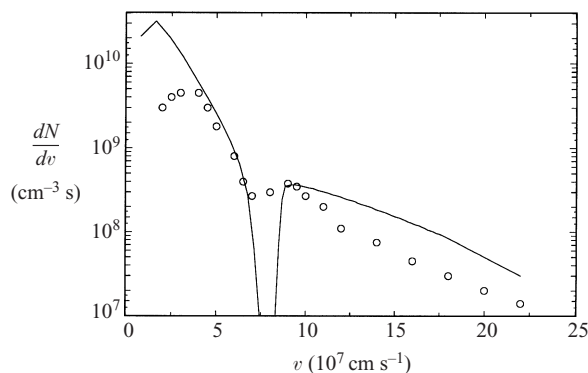
Figure 4. The spectrum of ions emitted from a solid Al target, irradiated by a 1.5 ps FWHM p-polarized Gaussian Nd-laser pulse with a peak laser intensity $10^{16}\,\mathrm{W\,cm^{-2}}$, incident at a 45° angle. The calculated data (curves) are compared with the experimental spectrum (Andreev *et al.* 1996), recorded at a 45° angle from the target normal (circles).

qualitatively similar to the measured spectrum. The number of high-energy ions in the experiment is reduced owing to the 45° angle of observation.

The spectrum of ions emitted normally from the target was measured in recent experiments by Komarov *et al.* (1997). In these experiments, a 1.5 ps FWHM Nd-laser pulse was incident at a 45° angle onto a plane Al target. The laser intensity was varied between 10^{16} and $10^{17}\,\mathrm{W\,cm^{-2}}$, and the intensity contrast was of the order of 10^{6}–10^{7}. The simulation results are presented here in greater detail. At the maximum of the laser pulse, the computed profiles of the plasma density and electric fields are plotted in Figs 5 and 6 for laser intensities of 10^{16} and $10^{17}\,\mathrm{W\,cm^{-2}}$. It should be noted that the small-scale oscillations in the density profile in Fig. 5 may be considered a numerical artefact, since they disappear when an artificial viscosity is introduced into the corona. On the other hand, the density profile in Fig. 6 shows a shock wave moving inwards, initiated by a laser-induced ponderomotive force. The narrow peak in Fig. 6 with a maximum density of about $27n_c$ is only 0.01λ wide. Similar shock waves were observed earlier in hydrodynamical simulations of interactions of intense picosecond pulses with solid targets (Kalashnikov *et al.* 1994).

Comparison of Figs 5 and 6 shows that the increase in laser intensity leads to a considerable shortening of the electron density scale length at the critical surface. While the density profile is near to optimum for resonance absorption for the lower intensity, resonant absorption is less efficient for $I = 10^{17}\,\mathrm{W\,cm^{-2}}$. The structure of the electric fields should lead to electron acceleration normally to the target for the lower intensity. A much broader angular distribution of fast electrons is expected for the higher intensity, since the longitudinal field is decreased by wavebreaking and the density profile modification (see Fig. 6). A broad angular spectrum of fast electrons should lead to fast-ion emission into a wide cone. The computed ion spectrum is presented in Fig. 7 for the respective intensities. The experimental ion spectrum, measured for the higher intensity, is normalized in the same way as in Fig. 4. Excellent agreement of the computed fast-ion energy and spectrum with experiment is obtained. The minimum in the experimental ion distribution is observed inside the velocity gap in the computed spectrum, which supports the
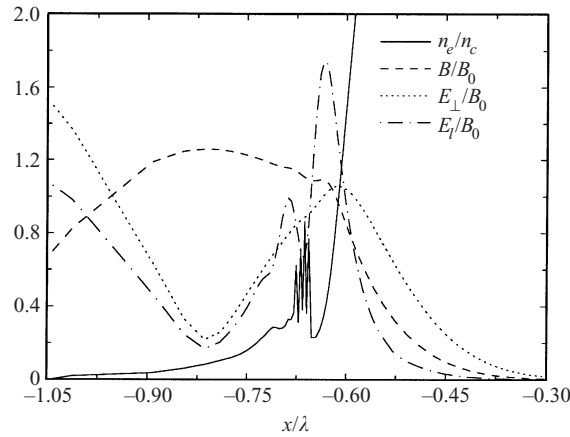
Figure 5. Profiles of the plasma density and of the laser fields at the peak $I = 10^{16}\,\mathrm{W\,cm^{-2}}$ of a 1.5 ps Gaussian pulse of p-polarized Nd-laser radiation, incident at a $45°$ angle on a solid Al target. B_0 is the amplitude of the incident laser magnetic field in vacuum.
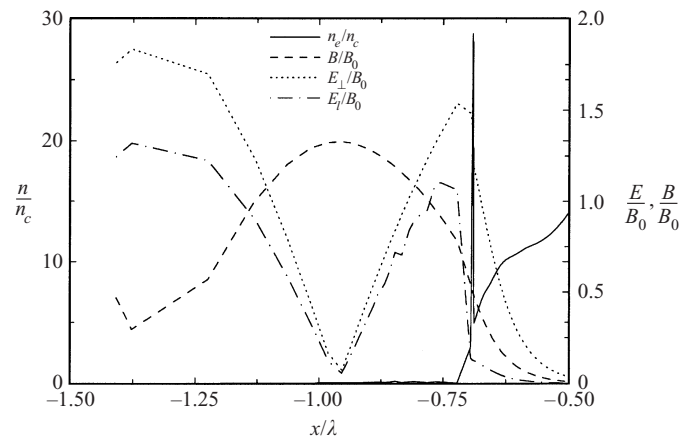

Figure 6. Profiles of the plasma density and of the laser fields at the peak $I = 10^{17}\,\mathrm{W\,cm^{-2}}$ of a 1.5 ps Gaussian pulse of p-polarized Nd-laser radiation, incident at a $45°$ angle on a solid Al target. B_0 is the amplitude of the incident laser magnetic field in vacuum.

model of ion acceleration. It also implies a reasonable agreement of the computed electron distribution with experiment.

As the applicability of our model has been demonstrated above, we now investigate the basic characteristics of the interactions. The laser absorption efficiency, plotted in Fig. 8, decreases slowly with laser intensity. The enhanced density profile modification due to the rising ponderomotive force leads not only to a decline in collisional absorption, but in our case also to a slight reduction in resonance absorption. However, the dynamics of the plasma corona is very complicated for the highest intensity studied here. In this case, there are periods when the plasma density profile changes rapidly and cavitons are formed. This leads to fast temporal variations in the absorption efficiency, and the overall absorption efficiency is also influenced. In this case, non-negligible variations of the overall absorption efficiency are observed when the detailed parameters of the simulations are modi-
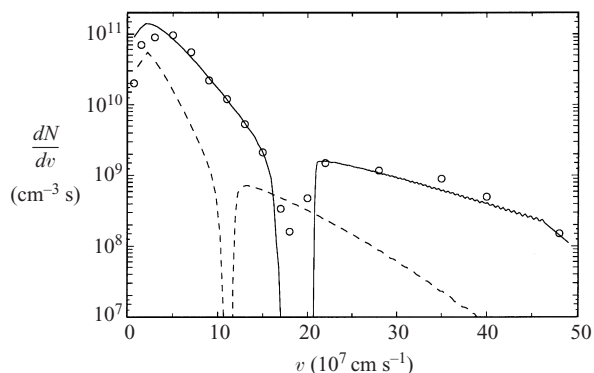
Figure 7. The spectrum of ions emitted normally from a solid Al target, irradiated by a 1.5 ps FWHM p-polarized Gaussian Nd-laser pulse incident at a $45°$ angle. The peak laser intensities are 10^{16} W cm^{-2} (dashed curves) and 10^{17} W cm^{-2} (solid curves). The data calculated for the higher intensity are compared with experiment (Komarov *et al.* 1997) (circles).
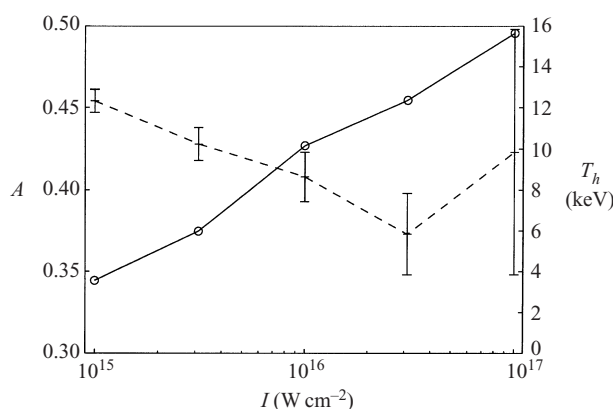

Figure 8. Laser absorption efficiency A (dashed line) and hot-electron temperature T_h (solid line) versus peak laser intensity. A p-polarized 1.5 ps FWHM Gaussian Nd-laser pulse is incident at a $45°$ angle onto a solid Al target.

fied. This uncertainty in the absorption efficiency is represented by the error bars in Fig. 8. The absorption efficiencies, calculated here, are somewhat lower than in experiments and in some PIC simulations; see the review by Gibbon and Förster (1996). This implies that it is rather difficult to account precisely for all the absorption mechanisms of ultrashort laser pulses in the frame of a 1D hydrocode. The same figure depicts the rise of the hot-electron temperature with laser intensity. The deduced scaling is $T_h \propto I^\alpha$, where $\alpha \propto 0.6$. This scaling is in good agreement with the scalings, observed in the PIC simulations (Gibbon and Bell 1992) and experimentally (Meyerhofer *et al.* 1993).

The energy of fast-ion emission grows with laser intensity, but the efficiency of laser energy conversion to fast-ion emission, displayed in Fig. 9, decreases. This behaviour is explained by the fact that the energy of the fast ions is proportional to the hot-electron temperature $T_h \propto I^\alpha$ with $\alpha < 1$. However, if energy transformation to a group of very fast and rather monoenergetic ions is preferred then the energy transformation increases very rapidly with laser intensity. Such growth is
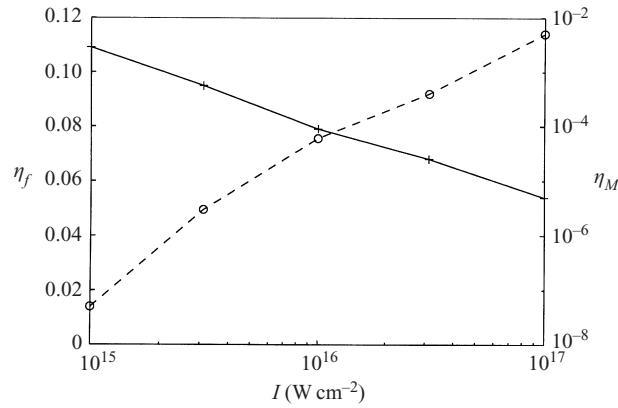
Figure 9. The efficiency η_f of laser energy transformation to the energy of fast ions (solid line) and the efficiency η_M of energy transformation to ions in the energy range 800–1000 keV (dashed line) versus peak laser intensity. A p-polarized 1.5 ps FWHM Gaussian Nd-laser pulse is incident at a 45° angle onto a solid Al target.

demonstrated in Fig. 9 for Al ions in the energy range 800–1000 keV. Thus high laser intensities are preferable for the generation of intense beams of high-energy ions for applications. However, the validity of our model is limited to laser intensities $I\lambda^2 < 10^{18}\,\mathrm{W\,cm^{-2}\,\mu m^2}$. For higher laser intensities, the ponderomotive pressure is expected to induce an inwards motion of the critical surface and of the coronal plasma during the main part of the laser pulse. This should significantly reduce ion acceleration by the ambipolar field. Thus we deduce that the optimum intensity for the ambipolar acceleration of high-energy ions is around $I \approx 10^{17}\,\mathrm{W\,cm^{-2}}$, and the transformation efficiency of the laser energy into the emission of high-energy ions may reach about 1%. Such an efficiency, though not very high, is acceptable because of unique properties of the source. The target surface emitting ions is very small, an ultrashort intense pulse of energetic ions is formed, and a high repetition rate is achievable.

4. Conclusions

A simplified, but self-consistent, one-dimensional hydrodynamical model has been developed for the description of ion emission from picosecond laser plasmas. It includes resonance absorption, fast-electron acceleration by resonance absorption, fast-electron transport into the solid target, and ion acceleration by the ambipolar electrostatic field. Simulations have been performed for the conditions of the published experiments (Meyerhofer *et al.* 1993; Andreev *et al.* 1996; Komarov *et al.* 1997), where the ion energy spectra were measured. Good agreement of simulations with the experimental results has been shown.

We have analysed the possibility of efficient laser energy conversion to high-energy ions, and have found an optimum laser intensity for the generation of MeV ions by picosecond laser pulses.

References

Ammosov, M. V., Delone, N. B. and Krainov, V. P. 1986 *Zh. Eksp. Teor. Fiz.* **91**, 2008 [*Soviet Phys. JETP* **64**, 1191].

Andreev, N. E., Silin, V. P. and Stenchikov, G. L. 1980 *Zh. Eksp. Teor. Fiz.* **78**, 1396.

Andreev, N. E., Auer, G., Baumgärtel, K. and Sauer, K. 1981 *Phys. Fluids* **24**, 1492.

Andreev, A. A., Limpouch, J. and Semakhin, A. N. 1994 *Izv. Akad. Nauk, Ser. Fiz.* **58**, 167 [*Bull. Russ. Acad. Sci.: Phys.* **58**, 1056].

Andreev, A. A., Bayanov, V. I., Vankov, A. B., Kozlov, A. A., Komarov, V. M., Kurnin, I. V., Solovyev, N. A., Chizhov, S. A., Yashin, V. E. and Limpouch, J. 1996 *Proc. SPIE* **2770**, 82.

Brown, I. G. 1989 *The Physics and Technology of Ion Sources*, Chap. 14. Wiley, New York.

Brunel, F. 1987 *Phys. Rev. Lett.* **59**, 52.

Davis, J., Clark, R. and Guiliani, J. 1995 *Laser Particle Beams* **13**, 3.

Dragila, R. and Gamaly, E. G. 1991 *Phys. Rev.* **A44**, 6828.

Dragila, R. and Krepelka, J. 1978 *J. Phys. (Paris)* **39**, 617.

Estabrook, K., Valeo, E. J. and Kruer, W. 1975 *Phys. Fluids* **18**, 1151.

Gibbon, P. and Bell, A. R. 1992 *Phys. Rev. Lett.* **68**, 1535.

Gibbon, P. and Förster, E. 1996 *Plasma Phys. Contr. Fusion* **38**, 769.

Gurevich, A. B. and Mescherkin, A. P. 1981 *Zh. Eksp. Teor. Fiz.* **80**, 1810.

Kalashnikov, M. P., Nickles, P. V., Schlegel, T., Schneurer, M., Billhardt, F., Will, I., Sandner, W. and Demchenko, N. N. 1994 *Phys. Rev. Lett.* **73**, 260.

Komarov, V. A., Borodin, V. G., Charukchev, A. V., Chernov, V. N., Iljin, V. V., Malinov, A. V., Migel, V. M. and Nikitin, N. V. 1997 In: *Book of Abstracts, Laser Interactions and Related Plasma Phenomena, Monterey, CA*, p. 38.

Lee, Y. T. and More, R. M. 1984 *Phys. Fluids* **27**, 1273.

Lee, R. W., Whitten, B. L. and Stout, R. E. 1984 *J. Quantitat. Spectrosc. Radiat. Transfer* **32**, 91.

Matte, J. P., Kieffer, J. C., Ethier, S., Chaker, M. and Peyrusse, O. 1994 *Phys. Rev. Lett.* **72**, 1208.

Meyerhofer, D. D., Chen, H., Delettrez, J. A., Soom, B., Uchida, S. and Yaakobi, B. 1993 *Phys. Fluids* **B5**, 2584.

Price, D. F., More, R. M., Walling, R. S., Guethlein, G., Shepherd, R. L., Stewart, R. E. and White, W. E. 1995 *Phys. Rev. Lett.* **75**, 252.

Rae, S. C. and Burnett, K. 1991 *Phys. Rev.* **A44**, 3835.

Sherwood, T. R. 1992 *Rev. Sci. Instrum.* **63**, 2789.

Wickens, L. M., Allen, J. E. and Rumsby, P. T. 1978 *Phys. Rev. Lett.* **41**, 243.